(This is a sample cover image for this issue. The actual cover is not yet available at this time.)

Remote Sensing of Environment 124 (2012) 299–309

Contents lists available at SciVerse ScienceDirect

Remote Sensing of Environment

journal homepage: www.elsevier.com/locate/rse

Polarized infrared emissivity of 2D sea surfaces with one surface reflection

Hongkun Li *, Nicolas Pinel, Christophe Bourlier

Lunam Université - Université de Nantes - IETR Laboratory, Polytech Nantes, Rue C. Pauc, La Chantrerie, BP 50609, 44306 Nantes Cedex 3, France

ARTICLE INFO

Article history:
Received 19 December 2011
Received in revised form 19 April 2012
Accepted 20 May 2012
Available online xxxx

Keywords:
Infrared emissivity
Sea surface
Surface reflection
Non-Gaussian

ABSTRACT

Sea surface infrared emissivity is an important parameter in oceanic remote sensing. This article derives the infrared emissivity of two-dimensional (2D) sea surfaces with an analytical model, where one surface reflection (surface-emitted surface-reflected) is considered. Polarization is studied, and the surface slope probability density function is Gaussian and then non-Gaussian to study the skewness and the kurtosis effects. It is shown that sea surface infrared emissivity is sensitive to the zenith observation angle and the wind direction, and the skewness and the kurtosis effects are significant for grazing directions (with zenith angle $>80°$). For Gaussian surfaces, surface emissivity for grazing zenith angles reaches maxima in the up-wind and down-wind directions, whereas minima are found in the cross-wind direction. After taking into account the skewness and the kurtosis effects, the surface emissivity has the largest value in the down-wind direction. The analytical results are then compared with measurements, which shows that considering one surface reflection significantly improves the agreement for large zenith angles.

1. Introduction

Sea surface infrared emissivity in the atmospheric transmission windows is an important parameter in oceanic remote sensing, e.g. for deriving the sea surface temperature. Sea surface infrared emissivity is nearly constant for observation directions near zenith, but it varies significantly with the observation angle measured from zenith (named zenith angle). In these observation directions, shadowing and surface reflections become significant, increasing the difficulty in predicting the sea surface emissivity with accuracy.

Early models of sea surface infrared emissivity derived the emissivity without considering sea surface reflections (named direct emissivity, or zero-order emissivity contribution). By contrast, the shadowing effect was usually considered. Masuda et al. (1988) calculated the unpolarized sea surface infrared emissivity by modeling the sea as a two-dimensional (2D) surface with Gaussian surface slope distribution. A normalization factor was used to estimate the shadowing effect. Instead of using the normalization factor, Yoshimori et al. (1994, 1995) took the shadowing effect into account in their emissivity model by using the Smith illumination function[1] (Smith, 1967). Freund et al. (1997) calculated the sea surface emissivity by an hemispherical ensemble average. Bourlier (2005) took a step forward by considering a non-Gaussian surface slope distribution introduced by Cox and Munk (1954), which takes the skewness and kurtosis effects into account.

However, Smith et al. (1996) reported a difference of about 0.02–0.03 between the measurements and the direct emissivity model of Masuda et al. (1988) for a zenith angle of 73.5°, because surface reflections were ignored. The model of Watts et al. (1996) and that of Wu and Smith (1997) both defined an empirical cutoff angle to calculate the surface-emitted surface-reflected emissivity (SESR, or named first-order emissivity contribution, as one reflection is considered). Because of the difficulty in defining the cutoff angle, the result has a large uncertainty. The model of Henderson et al. (2003) developed a ray-tracing Monte Carlo algorithm to calculate the sea surface emissivity with up to 10 surface reflections. This method may be a valuable reference, but it needs a long computation time. Masuda (2006) took into account the first-order emissivity contribution (SESR) by using a weighting function, which avoided defining an exact cutoff angle. More rigorously, Bourlier (2006) evaluated the first-order emissivity contribution by developing a first-order illumination function (with one reflection), which estimates the probability that a surface-emitted ray is reflected once by another point of the surface into the observation direction. The model of Masuda (2006) and that of Bourlier (2006) are analytical models, but they do not agree well with the results of the ray-tracing Monte Carlo method (Li et al., 2011b). Nalli et al. (2008) shared the idea of Masuda (2006) which used a weighting function to calculate the first-order emissivity contribution, but replaced the shadowing term used in Masuda (2006) by that of Saunders (1968). The most recent model was developed by Li et al. (2011b), in which one surface reflection was considered. They showed that the agreement with measurements is greatly improved by considering one surface reflection.

* Corresponding author. Tel.: +33 240 683 264; fax: +33 240 683 233.
E-mail address: hongkun.li@etu.univ-nantes.fr (H. Li).

[1] The illumination function was originally called "shadowing" function (Smith, 1967; Wagner, 1967). But as the word "shadowing" leads to confusion when surface reflections are considered, more recent models named it "illumination" function (Bourlier, 2006; Li et al., 2011a).

0034-4257/$ – see front matter © 2012 Elsevier Inc. All rights reserved.
doi:10.1016/j.rse.2012.05.021

Most of the above models do not take polarization into account, except for the models of Henderson et al. (2003) and Li et al. (2011b). It is reported that surface emissions are usually partially polarized (Shaw, 1999; Shaw & Marston, 2000) and Shaw and Marston (2000) calculated the degree of polarization (DOP) of the direct infrared emissivity of the sea surface. Li et al. (2011b) calculated the DOP of the sea surface infrared emissivity with one surface reflection, but the sea surface was considered as one-dimensional (1D), making the model less general.

In this paper, the sea surface infrared emissivity is determined, by taking both the zero- (direct) and first-order (SESR) emissivity contributions into account. The zero-order emissivity contribution is calculated following the model of Bourlier (2005), where the Smith illumination function (Smith, 1967) is used. When deriving the first-order contribution, we extend the model of Li et al. (2011b) to a two-dimensional (2D) sea surface. Polarization is taken into account and carefully dealt with, and the DOP is calculated. Moreover, the skewness and kurtosis effects are considered, following the mathematical development of the sea surface slope probability density function (PDF) given by Cox & Munk (1954) and Bourlier (2005). When deriving the sea surface infrared emissivity, the geometric optics approximation is assumed to be valid, as the infrared wavelengths are very small compared with the sea surface roughness (Li et al., 2011b).

This paper is organized as follows: in Section 2, the zero-order infrared emissivity contribution of 2D sea surfaces is calculated, with polarization taken into account, and in Section 3, the first-order emissivity contribution is derived. The numerical calculation results are shown in Section 4 and are compared with measurements.

2. Emissivity without reflection ε_0

The sea surface infrared emissivity without reflection, which is shown in Fig. 1, corresponds to the emission energy propagating directly toward the sensor situated in the observation direction (θ, ϕ), where θ is the zenith angle and ϕ is the azimuth angle measured from the up-wind direction. It is also called the zero-order emissivity contribution, as no surface reflection occurs. Models of zero-order sea surface infrared emissivity are well known (Bourlier, 2005; Freund et al., 1997; Masuda et al., 1988; Yoshimori et al., 1994, 1995). This section follows the work of Bourlier (2005) to derive the zero-order infrared emissivity contribution of 2D sea surfaces. In addition, polarization is taken into account.

2.1. Zero-order illumination function

As pointed out by several authors (Bourlier, 2005; Masuda et al., 1988; Smith, 1967), for large zenith angles θ, not all parts of the sea surface can be "seen" by the sensor, because of the surface roughness. Parts of the surface lie in shadow, as illustrated in dashed line in Fig. 1.

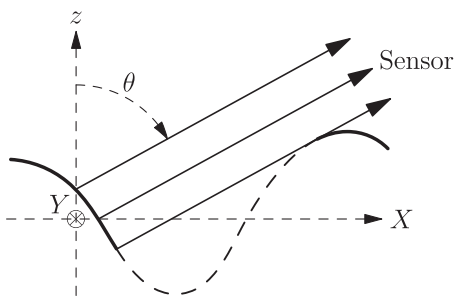

Fig. 1. Shadowing of the sea surface. The dashed part of the surface lies in the shadow for the sensor. The sensor is situated in the (θ, ϕ) direction, where ϕ is not shown. The X direction is the horizontal direction toward the sensor.

Shadowing is too significant to be ignored for large θ. As a result, a zero-order illumination function is used to estimate the probability that an arbitrary point of the sea surface, named M_0, is viewed by the sensor. Following Bourlier (2005), we employ the zero-order illumination function of Smith (1967). For more details, the reader is referred to Smith (1967) and Bourlier (2005). It is given by:

$$S_0(\theta, \gamma_X, \zeta_0) = \Upsilon(\mu - \gamma_X) F(\zeta_0)^{\Lambda(\mu)}, \tag{1}$$

where γ_X is the slope of M_0 with respect to the X direction (X is the horizontal direction toward the sensor, see Fig. 2), and ζ_0 is the height. $F(\zeta)$ is the surface height cumulative density function, given by:

$$F(\zeta) = \int_{-\infty}^{\zeta} p_{\zeta}(t)\mathrm{d}t, \tag{2}$$

where $p_{\zeta}(t)$ is the probability density function (PDF) of the surface height. The function $\Lambda(\mu)$ is related to the slope of the emission ray $\mu = cot\theta$ with respect to the X direction, given by (Bourlier, 2005, 2006; Smith, 1967):

$$\Lambda(\mu) = \frac{1}{\mu}\int_{\mu}^{+\infty} (\gamma_X - \mu) p_{\gamma}(\gamma_X)\mathrm{d}\gamma_X, \tag{3}$$

where $p_{\gamma}(\gamma_X)$ is the marginal surface slope probability density function (PDF) along the X direction. The function $\Upsilon(\mu - \gamma_X)$ is the unit step function, which equals 1 for $\gamma_X < \mu$ and 0 otherwise, meaning that all surface points with slope γ_X larger than the slope μ of the incidence ray are in shadow.

Averaging Eq. (1) over the heights ζ_0 of M_0 leads to the height-averaged zero-order illumination function, given by (Bourlier, 2005; Yoshimori et al., 1994):

$$\bar{S}_0(\theta, \gamma_X) = \frac{1}{1 + \Lambda(\mu)} \Upsilon(\mu - \gamma_X). \tag{4}$$

Eq. (4) holds for any surface height PDF. As the surface emissivity does not depend on the heights, the height-averaged illumination function is always used.

2.2. Rotation angle introduced by 2D surfaces

Fig. 2 shows the tangent plane of an arbitrary point M_0 of the sea surface with unitary normal vector $\hat{n}_0$.[2] The $\hat{x}$ direction is the up-wind direction, and the $\hat{y}$ direction is the cross-wind direction. The vector $\hat{z}$ points to the zenith. The sensor is located in the direction $\hat{s}(\theta, \phi)$, with θ being the zenith angle and ϕ being the azimuth angle measured from the up-wind direction. For convenience, a new coordinate system XY is defined by rotating anticlockwise the basis xy through an angle ϕ about the z axis, so that the sensor lies in the Xz plane. For short, xyz is the coordinate system related to the wind direction, and XYz is the one associated to the sensor direction.

The local plane of incidence[3] of M_0 is defined by the local normal to the tangent plane $\hat{n}_0$ and the observation direction $\hat{s}$. The angle χ_0 between $\hat{n}_0$ and $\hat{s}$ is the local incidence angle. The local horizontal polarization (denoted h_0, the electric vector is perpendicular to the local plane of incidence) and local vertical polarization (denoted v_0, the electric vector is parallel to the local plane of incidence) are defined. The unitary vector $\hat{u}_{v_0}$ of the v_0 polarization direction belongs to the local plane of incidence and is perpendicular to $\hat{s}$, and points upward of the tangent plane. The unitary vector $\hat{u}_{h_0}$ of the h_0 polarization direction is perpendicular to the local plane of incidence and

[2] In this paper, the symbol ˆ represents unitary vectors.

[3] This paper uses the term "plane of incidence" even though there is no incidence ray. The emission ray is treated as if it were generated by a specular reflection of an incidence ray, where the plane of incidence is defined.

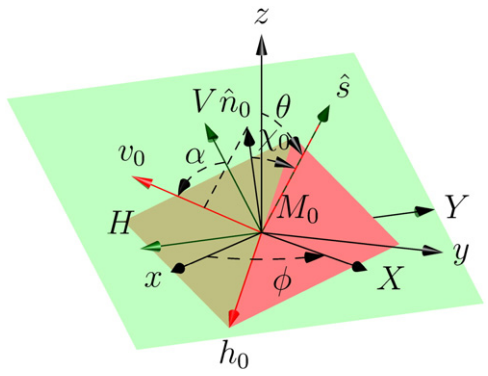

Fig. 2. The tangent plane of an arbitrary point M_0 (red) of the sea surface, with a unitary normal $\hat{n}_0$. The sensor is located in the $\hat{s}(\theta,\phi)$ direction. The light-green plane crosses point M_0 and is perpendicular to $\hat{s}$. The normal to the tangent plane $\hat{n}_0$ and the direction of observation $\hat{s}$ define the local plane of incidence, as well as the local incidence angle χ_0, and the local horizontal h_0 and vertical v_0 polarizations. The normal to the averaged surface (horizontal plane) $\hat{z}$ and $\hat{s}$ define the global plane of incidence, as well as the global horizontal H and vertical V polarizations. When $\hat{n}_0$ is different from $\hat{z}$, there is an angle α between the corresponding local and global polarization directions.

checks the relation $\hat{u}_{v_0} \times \hat{u}_{h_0} = \hat{s}$. As the slope of M_0 is arbitrary, the direction of the local normal vector $\hat{n}_0$ is arbitrary, as well as the local polarization directions.

To describe the polarization state of the sea surface infrared emissivity of the sea surface, the average sea surface is considered, which is parallel to the horizontal plane (XY or xy). The normal vector $\hat{z}$ to the average plane and the propagation direction $\hat{s}$ of the emission ray define the global plane of incidence. The global horizontal polarization (denoted H) and global vertical polarization (denoted V), as well as the corresponding unitary vectors $\hat{u}_V$ and $\hat{u}_H$, are defined in the same way as the local ones, by replacing the local normal vector $\hat{n}_0$ with the global one $\hat{z}$. The global polarization directions are fixed by the observation direction $\hat{s}$ and the zenith direction $\hat{z}$.

Generally, the tangent plane of an arbitrary surface point is not identical to the average sea surface (horizontal plane), which means that the local normal vector $\hat{n}_0$ is not identical to the $\hat{z}$ direction. As a result, the local plane of incidence is generally not identical to the global one. As $\hat{u}_V$, $\hat{u}_H$, $\hat{u}_{v_0}$ and $\hat{u}_{h_0}$ are perpendicular to $\hat{s}$, they belong to the same plane (the light green plane in Fig. 2). However, as the tangent plane is "rotated" from the average sea surface, there is an angle α between the local and global planes of incidence, which equals the one between $\hat{u}_V$ and $\hat{u}_{v_0}$, or between $\hat{u}_H$ and $\hat{u}_{h_0}$ (see Fig. 2). As the local polarization directions differ from point to point, the intensity of the emission of local v_0 and h_0 polarizations should be projected onto the global V and H polarization directions when deriving the sea surface infrared emissivity. As a result, a part of the locally horizontally (or vertically) polarized energy may pass to vertical (or horizontal) polarization in a global point of view. This effect is named "cross polarization" for short here. "Cross polarization" never occurs when deriving the zero-order 1D sea surface infrared emissivity (Li et al., 2011b), because the local and global planes of incidence are always identical, which means α equals 0.

2.3. Derivation of the zero-order emissivity ε_0 contribution

To derive the polarized infrared emissivity of sea surfaces, the local emissivity of an arbitrary point M_0 is calculated firstly. The unitary normal vector to the point M_0 can be expressed as (Yoshimori et al., 1995; Bourlier, 2006):

$$\hat{n}_0 = \frac{1}{\sqrt{1+\gamma_{x_0}^2+\gamma_{y_0}^2}} \begin{bmatrix} -\gamma_{x_0} \\ -\gamma_{y_0} \\ 1 \end{bmatrix}, \tag{5}$$

where γ_{x_0} and γ_{y_0} are the slopes of the point M_0 with respect to x and y directions, respectively. The propagation direction of the emission ray $\hat{s}$ is defined by its zenith and azimuth angles, as:

$$\hat{s} = \begin{bmatrix} \sin\theta\cos\phi \\ \sin\theta\sin\phi \\ \cos\theta \end{bmatrix}. \tag{6}$$

Then, the local incidence angle χ_0 (the angle between $\hat{n}_0$ and $\hat{s}$) is given by (Bourlier, 2006):

$$\cos\chi_0 = \hat{n}_0 \cdot \hat{s} = \frac{\cos\theta - \left(\gamma_{x_0}\cos\phi + \gamma_{y_0}\sin\phi\right)\sin\theta}{\sqrt{1+\gamma_{x_0}^2+\gamma_{y_0}^2}}. \tag{7}$$

The local emissivity of the point M_0 of v_0 and h_0 polarizations is given by:

$$\varepsilon_{0,v_0,h_0}^{\text{local}} = 1 - \left|r_{v_0,h_0}(\chi_0)\right|^2, \tag{8}$$

where $r(\chi_0)$ is the Fresnel reflection coefficient:

$$\begin{aligned} r_v(\chi) &= \frac{n\cos\chi - \cos\chi'}{n\cos\chi + \cos\chi'}, \\ r_h(\chi) &= \frac{\cos\chi - n\cos\chi'}{\cos\chi + n\cos\chi'}, \end{aligned} \tag{9}$$

with n being the refraction index of the sea and χ' being the transmission angle given by Snell's law: $\sin\chi' = \sin\chi/n$.

To derive the polarized emissivity of the sea surface, the local emissivity of v_0 and h_0 polarizations is projected to the V and H polarization directions. The emissivity of v_0V (local v_0 polarization projected to global V polarization), v_0H, h_0V, and h_0H polarizations is given by:

$$\begin{aligned} \varepsilon_{0,v_0V} &= \varepsilon_{0,v_0}^{\text{local}}\cos^2\alpha \\ \varepsilon_{0,v_0H} &= \varepsilon_{0,v_0}^{\text{local}}\sin^2\alpha \\ \varepsilon_{0,h_0V} &= \varepsilon_{0,h_0}^{\text{local}}\sin^2\alpha \\ \varepsilon_{0,h_0H} &= \varepsilon_{0,h_0}^{\text{local}}\cos^2\alpha \end{aligned}, \tag{10}$$

where the square in $\cos^2\alpha$ and $\sin^2\alpha$ stands for the projection of intensity. The rotation angle α is derived in detail in Appendix A. The emissivity of global V and H polarizations is given by:

$$\begin{aligned} \varepsilon'_{0,V} &= \varepsilon_{0,v_0V} + \varepsilon_{0,h_0V} \\ \varepsilon'_{0,H} &= \varepsilon_{0,v_0H} + \varepsilon_{0,h_0H} \end{aligned}. \tag{11}$$

Following the method of Bourlier (2005), the zero-order infrared emissivity of the sea surface is given by:

$$\begin{aligned} \varepsilon_{0,V} &= \left\langle \varepsilon'_{0,V} g_0 \bar{S}_0 \right\rangle_0 \\ \varepsilon_{0,H} &= \left\langle \varepsilon'_{0,H} g_0 \bar{S}_0 \right\rangle_0 \end{aligned}, \tag{12}$$

where $\bar{S}_0$ is the height-averaged zero-order illumination function given by Eq. (4), and the function g_0 results from projecting the area around the point M_0 onto the direction perpendicular to the observation direction, given by:

$$g_0 = 1 - \left(\gamma_{x_0}\cos\phi + \gamma_{y_0}\sin\phi\right)\tan\theta. \tag{13}$$

The symbol $\langle\cdots\rangle_0$ stands for the statistical average over the slopes of M_0, given by:

$$\langle\cdots\rangle_0 = \int_{-\infty}^{+\infty}\int_{-\infty}^{+\infty}\cdots p\left(\gamma_{x_0},\gamma_{y_0}\right)\mathrm{d}\gamma_{x_0}\mathrm{d}\gamma_{y_0}, \tag{14}$$

where $p(\gamma_{x_0}, \gamma_{y_0})$ is the joint probability density function (PDF) of the slopes of point M_0 with respect to the x and y directions.

For the ease of calculating the integrations in Eq. (14), the following changes of variables are performed (Bourlier, 2005):

$$\begin{aligned}\gamma_{x_0} &= \gamma_X cos\phi - \gamma_Y sin\phi \\ \gamma_{y_0} &= \gamma_X sin\phi + \gamma_Y cos\phi\end{aligned}, \tag{15}$$

where γ_X and γ_Y are the slopes of the point M_0 with respect to the X and Y directions, respectively. The integration variables in Eq. (14) become:

$$d\gamma_{x_0} d\gamma_{y_0} = J d\gamma_X d\gamma_Y, \tag{16}$$

where $J=1$ is the Jacobian of the changes of variables.

3. Emissivity with one surface reflection ε_1

Comparison with measurements showed that the zero-order models underestimate the sea surface infrared emissivity for large zenith angles θ (Li et al., 2011b; Watts et al., 1996; Wu & Smith, 1997). The reason is that the surface-emitted surface-reflected emissivity (SESR, first-order contribution) is not taken into account. Surface reflection effect is significant for large zenith angles θ. Fig. 3 shows that an emission ray from one point M_1 is reflected to the sensor by another point M_0 of the surface. This section extends the model of Li et al. (2011b) to 2D surfaces.

3.1. First-order illumination function

To evaluate the surface reflections, Li et al. (2011a) developed a first-order illumination function for 1D sea surfaces. In the same year, they derived the 1D sea surface infrared emissivity with the same illumination function (Li et al., 2011b). This article adopts this first-order illumination function, and extends it to 2D sea surfaces.

The first-order illumination function gives the probability that the emission ray from point M_1 is reflected specularly to the sensor by another point M_0 on the surface (see Fig. 3). In the model of Li et al. (2011a), the reverse ray path is used for better convenience, which assumes an emission ray from the sensor is reflected specularly by M_0 to M_1. This section follows the same procedure. The first-order illumination function is given by the probability that the ray $\hat{s}$ (the ray from M_0 to the sensor) does not reach the surface (with probability P_1) while the ray $-\hat{s}'$ (the ray form M_0 to M_1) reaches the surface at M_1 (with probability P_2). A new system of coordinates $X'Y'$ is defined in the same way as XY, by replacing M_0 with M_1 and the sensor with M_0.

The probability that the ray $\hat{s}$ does not reach the surface equals the zero-order illumination function, given by:

$$P_1 = \Upsilon(\mu - \gamma_X) F(\zeta_0)^{\Lambda(\mu)}. \tag{17}$$

However, the probability that the ray $-\hat{s}'$ reaches the surface is unknown. It depends on whether the ray $-\hat{s}'$ propagates upward or downward. If it propagates downward, it surely reaches the surface thus $P_2=1$; if it propagates upward, the probability that it reaches the surface equals the complementary probability that it does not. To conclude, P_2 is given by:

$$P_2 = \begin{cases} 1 & \text{if } \theta' > 90^\circ \\ 1 - F(\zeta_0)^{\Lambda_1(\mu_1)} & \text{if } \theta' < 90^\circ \end{cases}, \tag{18}$$

where μ_1 is the slope of the ray $\hat{s}'$ with respect to the X' direction. The function $\Lambda_1(\mu_1)$ is given by:

$$\Lambda_1(\mu_1) = \frac{1}{\mu_1} \int_{-\infty}^{\mu_1} (\gamma_{X'} - \mu_1) p_\gamma(\gamma_{X'}) d\gamma_{X'}, \tag{19}$$

where $p_\gamma(\gamma_{X'})$ is the marginal surface slope PDF with respect to the X' direction.

To sum up, the first-order illumination function for 2D surfaces is given by:

$$S_1(\theta, \gamma_X, \gamma_Y, \zeta_0) = \Upsilon(\mu - \gamma_X) F(\zeta_0)^{\Lambda(\mu)} \times \begin{cases} 1 & \text{if } \theta' > 90^\circ \\ 1 - F(\zeta_0)^{\Lambda_1(\mu_1)} & \text{if } \theta' < 90^\circ \end{cases} \tag{20}$$

The height-averaged first-order illumination function is obtained by averaging Eq. (20) over the height ζ_0, and is given by:

$$\bar{S}_1(\theta, \gamma_X, \gamma_Y) = \Upsilon(\mu - \gamma_X) \times \begin{cases} \dfrac{1}{1+\Lambda(\mu)} & \text{if } \theta' > 90^\circ \\ \dfrac{\Lambda_1(\mu_1)}{[1+\Lambda(\mu)][1+\Lambda(\mu)+\Lambda_1(\mu_1)]} & \text{if } \theta' < 90^\circ \end{cases}. \tag{21}$$

Eqs. (20) and (21) are the general forms of the first-order illumination function. For the axes X and X' in the same or the opposite directions, the 2D first-order illumination function equals the 1D one given by Li et al. (2011b).

3.2. Rotation angle β between local planes of incidence at M_0 and M_1

Fig. 4 shows two points M_1 and M_0 of the sea surface and their tangent planes. An emission ray $\hat{s}'$ propagates from M_1 to M_0, where it is then reflected specularly to the sensor. Unlike 1D surfaces, the propagation

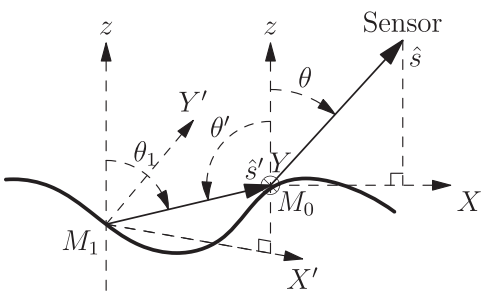

Fig. 3. The surface-emitted ray $\hat{s}'$ from M_1 is reflected by another surface point M_0 to the sensor in the $\hat{s}(\theta,\phi)$ direction.

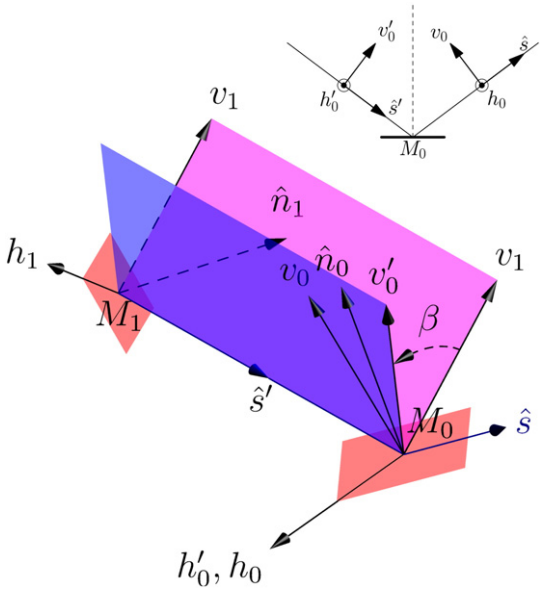

Fig. 4. The tangent planes (red planes) of points M_0 and M_1, and the local planes of incidence (blue plane for M_0, magenta plane for M_1).

direction of the emission ray $\hat{s}'$ and the normals to these two points are generally not in the same plane. As a result, the local planes of incidence (defined by $\hat{s}'$ and the local normals) of these two points are not identical, but differ with a rotation angle β, shown in Fig. 4. The angle β is derived in Appendix B.

The local horizontal and vertical polarizations (denoted as v_1 and h_1 to avoid confusion) of the emission ray from M_1 are defined in the same way as v_0 and h_0. The v_0' and h_0' directions are the local vertical and horizontal polarization directions of the incidence ray $\hat{s}'$ to the point M_0. Before calculating the reflection, the intensity of the emission of v_1 and h_1 polarizations should be projected to the v_0' and h_0' polarizations, which also leads to the so call "cross polarization."

3.3. Derivation of the first-order emissivity contribution ε_1

In this subsection, the sea surface infrared emissivity with one reflection is developed according to the slopes of the points M_0 and M_1 and the observation angle $\hat{s}(\theta,\phi)$.

To be consistent with the first-order illumination function, the reverse ray path is used, which assumes that the emission ray from the sensor reaches the surface at M_0 and is reflected specularly to M_1. Knowing the observation direction $\hat{s}$ and the slope of the point M_0, the unitary vector of the propagation direction of the reflection ray $-\hat{s}'$ is given by:

$$\hat{u}_{M_0M_1} = -\hat{s}' = 2\hat{n}_0(\hat{n}_0\cdot\hat{s})-\hat{s}. \tag{22}$$

The global reflection angle θ' is then given by:

$$cos\,\theta' = \hat{u}_{M_0M_1}\cdot\hat{z} = cos\,\theta\left[2g_0\left(1+\gamma_{x_0}^2+\gamma_{y_0}^2\right)^{-1}-1\right] \tag{23}$$

According to Eq. (6), the unitary vector $\hat{s}'$ can be denoted as $\hat{s}'(\theta_1,\phi_1)$, where θ_1 and ϕ_1 are given by:

$$\theta_1 = \mathrm{acos}(\hat{s}_z'), \tag{24}$$

$$cos\,\phi_1 = \hat{s}_x'/sin\,\theta_1, \tag{25}$$

$$sin\,\phi_1 = \hat{s}_y'/sin\,\theta_1. \tag{26}$$

The local incidence angle of the point M_1 is given in the same way as Eq. (7) by:

$$cos\chi_1 = \frac{cos\,\theta_1-\left(\gamma_{x_1}cos\,\phi_1+\gamma_{y_1}sin\,\phi_1\right)sin\,\theta_1}{\sqrt{1+\gamma_{x_1}^2+\gamma_{y_1}^2}}, \tag{27}$$

where γ_{x_1} and γ_{y_1} are the slopes of the point M_1 with respect to the x and y directions, respectively.

The local emissivity of v_1 and h_1 polarizations referring to the point M_1 is then given by:

$$\varepsilon_{1,v_1,h_1}^{\mathrm{local}} = 1-\left|r_{v_1,h_1}(\chi_1)\right|^2. \tag{28}$$

Before reflecting the ray specularly from $\hat{s}'$ to $\hat{s}$, the intensity of the emission of v_1 and h_1 polarizations should be projected to v_0 and h_0 polarizations, given by:

$$\begin{aligned}
\varepsilon_{1,v_1v_0'}^{\mathrm{local}} &= \varepsilon_{1,v_1}^{\mathrm{local}}cos^2\beta = \left[1-\left|r_{v_1}(\chi_1)\right|^2\right]cos^2\beta,\\
\varepsilon_{1,v_1h_0'}^{\mathrm{local}} &= \varepsilon_{1,v_1}^{\mathrm{local}}sin^2\beta = \left[1-\left|r_{v_1}(\chi_1)\right|^2\right]sin^2\beta,\\
\varepsilon_{1,h_1v_0'}^{\mathrm{local}} &= \varepsilon_{1,h_1}^{\mathrm{local}}sin^2\beta = \left[1-\left|r_{h_1}(\chi_1)\right|^2\right]sin^2\beta,\\
\varepsilon_{1,h_1h_0'}^{\mathrm{local}} &= \varepsilon_{1,h_1}^{\mathrm{local}}cos^2\beta = \left[1-\left|r_{h_1}(\chi_1)\right|^2\right]cos^2\beta.
\end{aligned} \tag{29}$$

After the reflection, the emissivity of v_0 and h_0 polarizations is given by:

$$\varepsilon_{1,p_1q_0}^{\mathrm{local}} = \varepsilon_{1,p_1q_0'}^{\mathrm{local}}\left|r_{q_0}(\chi_0)\right|^2, \tag{30}$$

where $p_1=\{v_1, h_1\}$, $q_0=\{v_0, h_0\}$.

To derive the polarized emissivity of the sea surface, the local emissivity is projected to the global polarization directions V and H as:

$$\varepsilon_{1,p_1,q_0,C} = \varepsilon_{1,p_1,q_0}^{\mathrm{local}}f(\alpha), \tag{31}$$

where $C=\{V, H\}$. The function $f(\alpha)=cos^2\alpha$ if q_0 and C are both horizontal and vertical polarizations. Otherwise, $f(\alpha)=sin^2\alpha$. The emissivity of V and H polarizations is given by:

$$\begin{aligned}
\varepsilon_{1,V}' &= \textstyle\sum_{p_1=\{v_1,h_1\},q_0=\{v_0,h_0\}}\varepsilon_{1,p_1,q_0,V},\\
\varepsilon_{1,H}' &= \textstyle\sum_{p_1=\{v_1,h_1\},q_0=\{v_0,h_0\}}\varepsilon_{1,p_1,q_0,V},
\end{aligned} \tag{32}$$

Compared with emissivity of 1D sea surfaces (see Eq. 29 of Li et al., 2011b), "cross polarization" terms, where p_0, q_0 and C do not represent the same polarization, appear here. For 1D surfaces, these terms never occur, as the angles α and β both equal 0.

Finally, the polarized emissivity of the sea surface is obtained by averaging $\varepsilon_{1,V}'$ and $\varepsilon_{1,H}'$ over the slopes of M_1 and M_0, given by (Li et al., 2011b):

$$\begin{aligned}
\varepsilon_{1,V} &= \left\langle\varepsilon_{1,V}'g_0\bar{S}_1\right\rangle_1,\\
\varepsilon_{1,H} &= \left\langle\varepsilon_{1,H}'g_0\bar{S}_1\right\rangle_1,
\end{aligned} \tag{33}$$

where $\bar{S}_1$ is the height-averaged first-order illumination function. The symbol $\langle\cdots\rangle_1$ stands for the statistical average over the slopes of M_1 and M_0:

$$\begin{aligned}
\langle\cdots\rangle_1 = &\textstyle\int_{-\infty}^{+\infty}\int_{-\infty}^{+\infty}\int_{-\infty}^{+\infty}\int_{-\infty}^{+\infty}\cdots\\
&p\left(\gamma_{x_1},\gamma_{y_1},\gamma_{x_0},\gamma_{y_0}\right)d\gamma_{x_1}d\gamma_{y_1}d\gamma_{x_0}d\gamma_{y_0},
\end{aligned} \tag{34}$$

where $p(\gamma_{x_1},\gamma_{y_1},\gamma_{x_0},\gamma_{y_0})$ is the joint PDF of the slopes of the points M_0 and M_1 with respect to the x and y directions.

To calculate the integration in Eq. (34), the changes of variables given by Eq. (15) are performed, as well as the following ones:

$$\begin{aligned}
\gamma_{x_1} &= \gamma_{X'}cos\,\phi_1-\gamma_{Y'}sin\,\phi_1\\
\gamma_{y_1} &= \gamma_{X'}sin\,\phi_1+\gamma_{Y'}cos\,\phi_1
\end{aligned}, \tag{35}$$

where $\gamma_{X'}$ and $\gamma_{Y'}$ are the slopes of the point M_1 with respect to the X' and Y' directions, respectively. In addition:

$$d\gamma_{x_1}d\gamma_{y_1}d\gamma_{x_0}d\gamma_{y_0} = d\gamma_{X'}d\gamma_{Y'}d\gamma_Xd\gamma_Y. \tag{36}$$

3.4. Surface slope PDFs of M_0 and M_1

The sea surface slope PDF $p_\gamma(\gamma_x,\gamma_y)$ is assumed to be either Gaussian or non-Gaussian, so as to evaluate the skewness and kurtosis effects. The non-Gaussian surface slope PDF was first introduced and specified by Cox & Munk (1954). Bourlier (2005) later derived the marginal slope PDF along the X direction, with which the functions $\Lambda(\mu)$ (Eq. 3) and $\Lambda_1(\mu_1)$ (Eq. 19) can be calculated. The details of the calculation are reported in Appendix C.

To carry out the integrations in Eq. (34), the joint PDF $p(\gamma_{x_0}, \gamma_{y_0}, \gamma_{x_1}, \gamma_{y_1})$ of the slopes of the surface points M_0 and M_1 must be determined, which is given by:

$$p\left(\gamma_{x_0}, \gamma_{y_0}, \gamma_{x_1}, \gamma_{y_1}\right) = p_\gamma\left(\gamma_{x_0}, \gamma_{y_0}\right) p\left(\gamma_{x_1}, \gamma_{y_1} \middle| \gamma_{x_0}, \gamma_{y_0}\right). \tag{37}$$

Knowing that $-\hat{s}'$ crosses the surface at M_1, the slope PDF of M_1 is posterior. Obviously, not all slopes of the sea surface can be the slopes of M_1, for example, the slopes leading to an unphysical local incidence angle $|\chi_1| > 90°$. As little information is available, the assumption of Li et al. (2011b) is used, which assumes that any slope fulfilling the condition $|\chi_1| < 90°$ may equally be the slope of M_1. According to Eq. (27), the following condition is then obtained:

$$\cos\theta_1 - \left(\gamma_{x_1}\cos\phi_1 + \gamma_{y_1}\sin\phi_1\right)\sin\theta_1 > 0, \tag{38}$$

or equally:

$$\gamma_{X'} < \mu_1. \tag{39}$$

The slope PDF of the point M_1 is then given by:

$$p\left(\gamma_{x_1}, \gamma_{y_1} \middle| \gamma_{x_0}, \gamma_{y_0}\right) = \frac{\Upsilon(\mu_1 - \gamma_{X'})}{\int_{-\infty}^{\mu_1} p_\gamma(t)\mathrm{d}t} p_\gamma\left(\gamma_{x_1}, \gamma_{y_1}\right), \tag{40}$$

where $p_\gamma(t)$ is the marginal surface slope PDF along the X' direction.

4. Numerical results

In this section, we present calculations based upon the zero- and first-order components of sea surface infrared emissivity developed in Sections 2 and 3. The calculation is performed for wavelengths inside the infrared atmospheric windows of 3–5 μm and 8–13 μm. The sea refraction index n in these regions is given by Hale & Querry (1973), for example, $n = \{1.3510 + 0.0046i;\ 1.2180 + 0.0508i\}$ for wavelengths $\lambda = \{4;\ 10\}$ μm. We recall that Hale and Querry (1973) did not take salinity into account.

4.1. Emissivity without reflection ε_0

The polarized zero-order contribution of sea surface infrared emissivity ε_0 (direct emissivity) is calculated according to Eq. (12). It is recalled that the polarization state of the sea surface infrared emissivity is measured by the global horizontal and vertical polarizations, which are defined referring to the average sea surface.

Fig. 5(a) shows the zero-order emissivity contribution ε_0 of h_0H, h_0V, v_0H and v_0V polarizations (the terms of the right-hand side of Eq. (11)) for the wavelength $\lambda = 4$ μm. The sensor is located in the up-wind direction ($\phi = 0°$). The wind speed u_{12} at 12.5 m above the sea surface equals 10 m/s. The sensor is located in the up-wind direction ($\phi = 0°$), and the surface slope PDF is assumed to be Gaussian. The results for other ϕ and the ones for a non-Gaussian slope PDF are also calculated, which are not shown as they have similar trends and lead to the same conclusion.

It is shown that the "cross polarization" terms (h_0V and v_0H) are significant only for small zenith angles, e.g. $\theta < 30°$. These terms decrease rapidly with the increase of the zenith angle θ and are rather small for large zenith angles: for instance, $\varepsilon_{0,h_0V} \approx 0.0134$ and $\varepsilon_{0,v_0H} \approx 0.0177$ for $\theta = 85°$. On the other hand, the terms ε_{0,h_0H} and ε_{0,v_0V} are always strong.

To give an explanation to the rapid decrease of the "cross polarization" terms, the average of the rotation angle α, given by $<\alpha\bar{S}_0>_0$, is calculated for both Gaussian and non-Gaussian surface slope PDFs. The angle α is derived in Appendix A. The illumination function $\bar{S}_0$ is taken into account to eliminate the influence of the points in shadow, which does not contribute to the observed emissivity. The result is shown in Fig. 5(b). It is shown that the average of α decreases with the increase of θ, from slightly over 40° for $\theta = 0°$ to about 0° for $\theta = 90°$. As a result, $\sin\alpha$ decreases rapidly as θ increases, and the cross polarization terms vanish (see Eq. 10).

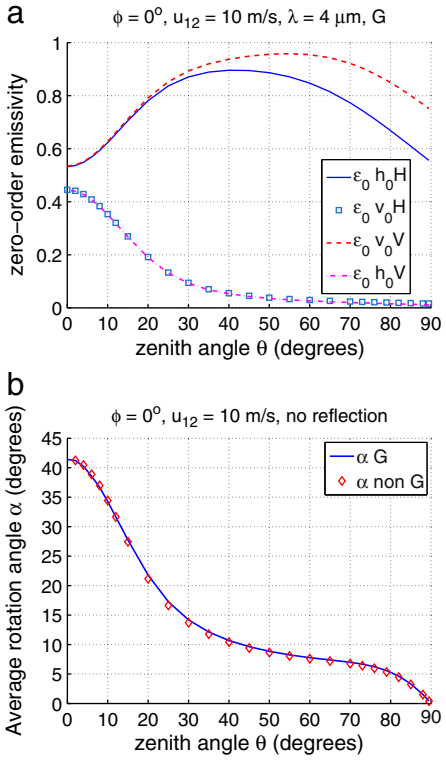

Fig. 5. Sea surface zero-order emissivity contribution of v_0V, h_0V, h_0H and v_0H polarizations (a) and the average rotation angle $<\alpha\bar{S}_0>_0$ (b). The sensor is located in the up-wind direction ($\phi = 0°$).

The zero-order contribution of sea surface infrared emissivity of global H and V polarizations is calculated for both Gaussian and non-Gaussian sea surface slope PDF, with the same parameters as in Fig. 5, using Eq. (11). The result is then compared with that of Li et al. (2011b), which considers 1D surfaces with Gaussian slope PDF, shown in Fig. 6.

It is shown in Fig. 6(a) that the zero-order emissivity contributions of 1D or 2D surfaces and with Gaussian or non-Gaussian surface slope PDFs have similar trends. The surface emissivity of H polarization decreases with the increase of θ, while the one of V polarization increases to a maximum value and then decreases, because of the Brewster angle ($\theta_B \approx 53°$ for $\lambda = 4$ μm, flat surface). The difference between the emissivity of 1D and 2D surfaces with Gaussian slope PDF is relatively small (see Fig. 6(b), solid and dashed lines). The maxima of the difference occur for $\theta = 90°$, of absolute value about 1.1×10^{-3} for H polarization and about 7.0×10^{-3} for V polarization. The difference between the 2D surface emissivities with Gaussian and non-Gaussian slope PDFs is also small, but becomes larger for large zenith angles $\theta > 85°$ (see Fig. 6(b), dashed-dotted line and line with closed circle), meaning that the skewness and kurtosis effects become significant only in this region. The largest differences are also found for $\theta = 90°$, of absolute value about 1.9×10^{-2} for H polarization and about 1.6×10^{-2} for V polarization. The values of the difference vary with the wind direction ϕ.

4.2. Emissivity with one reflection ε_1

The first-order contribution of sea surface infrared emissivity (SESR) ε_1 is calculated by Eq. (33). The calculations are performed for 2D sea surfaces with Gaussian or non-Gaussian slope PDF, and

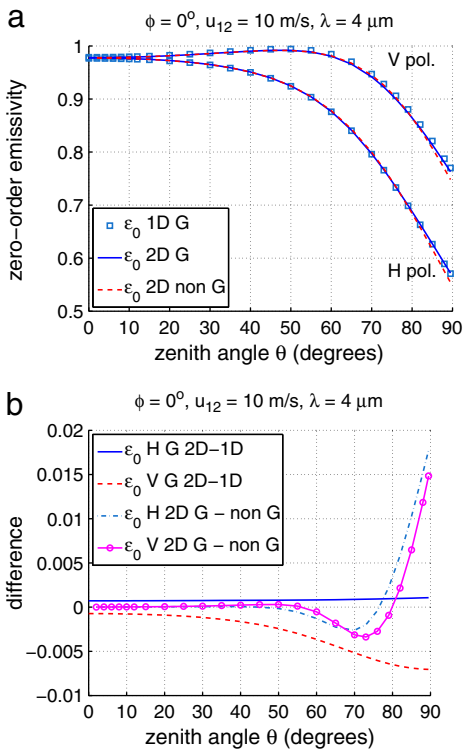

Fig. 6. (a) Polarized sea surface zero-order infrared emissivity ε. (b) The difference between the emissivities of 1D and 2D surfaces with Gaussian slope PDF, and the difference between the results of 2D surfaces with Gaussian and non-Gaussian slope PDFs. The sensor is located in the up-wind direction ($\phi=0°$).

are compared with the model of Li et al. (2011b). The results for the wind speed 10 m/s and the wavelength 4 μm are shown in Fig. 7.

It is shown that the first-order contribution of sea surface emissivity is significant for large zenith angles, e.g. $\theta>60°$. Maxima about 0.025 are found around $\theta=80°$. The first-order emissivity contributions of 1D and 2D surfaces (solid and dashed lines in Fig. 7) are similar. The surface emissivity of 2D surfaces of either H or V polarization is slightly smaller than that of 1D surfaces for large zenith angles $\theta>70°$.

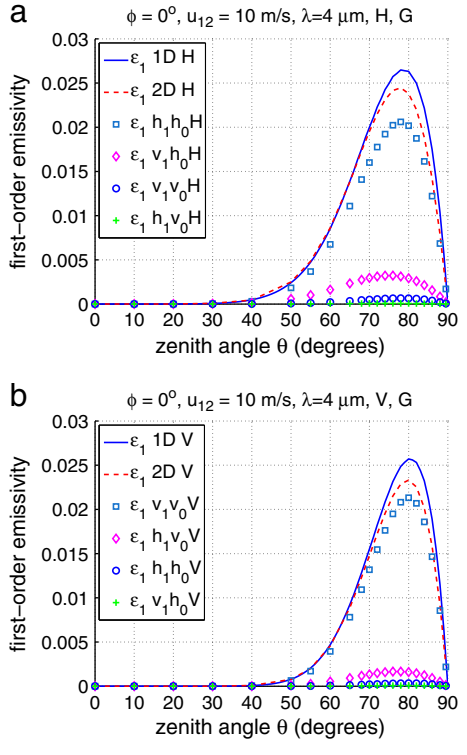

Fig. 7. First-order sea surface infrared emissivity of H polarization (a) and of V polarization (b). The sensor is located in the up-wind direction.

The "cross polarization" terms (terms where p_1, q_0 and C do not represent the same polarization) are very weak. The averages of the angles α and β are calculated, which are given by $<\alpha\bar{S}_1>_1$ and $<\beta\bar{S}_1>_1$. The first-order illumination function is taken into account so as to weight each α and β according to the corresponding probability of observing surface reflections. The result is shown in Fig. 8, with the same parameters as Fig. 7.

It is shown that the average values of α and β are very small, with maxima about 4° for β and 1.5° for α ($sin^2(4°)\approx 4.9\times10^{-3}$, $sin^2(1.5°)\approx 6.8\times10^{-4}$). In other words, the local and global polarization directions are almost the same; thus, the "cross polarization" terms are weak. In addition, as α and β are small, the local planes of incidence at the source point (M_0) and the reflection point (M_1), and the global plane of incidence are almost parallel with each other. As a result, only a narrow area of the sea surface around its intersection with the global plane of incidence participate in producing the first-order emissivity contribution.

Although a sensor can neither measure the emissivity of p_1q_0C polarization separately, nor measure the value of the rotation angles α and β, it is relevant to study the "cross polarization" effect. First of all, it help us understand better the physical process. Secondly, when the surface reflectivity is calculated, "cross polarization" can be measured.

Fig. 9 compares the polarized first-order emissivity contribution with Gaussian and non-Gaussian sea surface slope PDFs, with the same wind speed and wavelength as Fig. 7. Fig. 9(a) shows the first-order surface emissivity contribution with respect to the zenith angle θ. It is shown that in the up-wind direction ($\phi=0°$), the emissivity with non-Gaussian slope PDF is slightly larger for moderate zenith angles (e.g. $20°<\theta<60°$) and smaller for larger zenith angles (e.g. $\theta>60°$). The largest differences caused by the skewness and kurtosis effects are about 2.5×10^{-3}, which occurs around $\theta=75°$.

Fig. 9(b) shows the first-order surface emissivity contribution with respect to the azimuth angle ϕ. As it is symmetrical about $\phi=180°$, the part for $\phi\in[180°,360°]$ is not shown. The first-order emissivity contribution with Gaussian slope PDF, of H or V polarization, is nearly constant. However, the one with non-Gaussian slope PDF varies with ϕ. In other words, the emissivity with one surface reflection is more sensitive to the wind direction after taking the skewness and kurtosis effects into account. The first-order contribution with non-Gaussian slope PDF is minimum for $\phi=0°$, which is smaller than that with Gaussian slope PDF and checks the conclusion obtained previously in Fig. 9(a), and is maximum for $\phi=180°$, which is larger than that with Gaussian slope PDF.

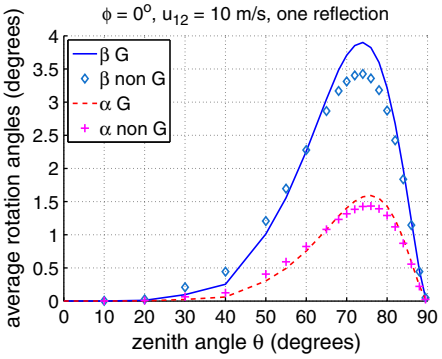

Fig. 8. Averaged α and β.

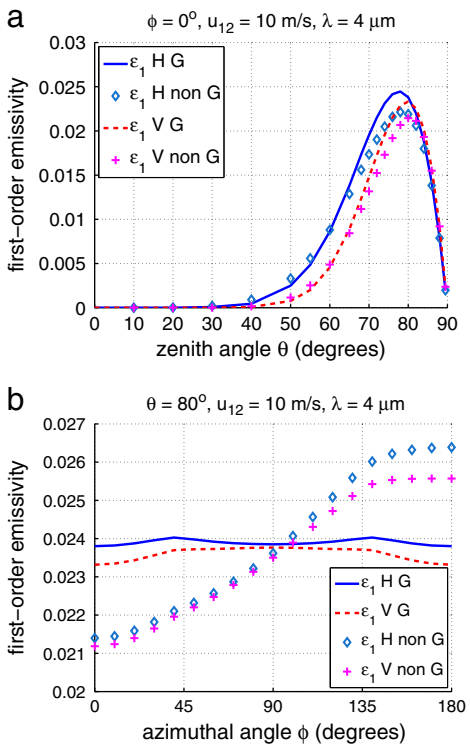

Fig. 9. Comparison of the first-order contribution of sea surface infrared emissivity with Gaussian and non-Gaussian slope PDF with respect to θ (a) and ϕ (b).

4.3. Total emissivity of the sea surface

As Li et al. (2011b) showed that emissivities with two and more reflections (second and higher order contributions, or SESRSR, ···) are negligible, the total emissivity of the sea surface is the sum of the zero- and first-order contributions, ε_0 and ε_1 respectively. Fig. 10 shows the zero-order contribution and the total polarized emissivities of the sea surface, with respect to the zenith angle θ and azimuth angle ϕ. The wind speed equals 10 m/s and the wavelength is 4 μm.

It is shown that the total sea surface infrared emissivity ($\varepsilon_0+\varepsilon_1$) is significantly increased after taking into account one surface reflection for large zenith angles, e.g. $\theta>60°$ (see Fig. 10(a)). It has larger values for $\phi=0°$, 180° than for $\phi=90°$ (see Fig. 10(b)), as the sea surface has a larger RMS slope in the up-wind (or down-wind) direction. The influence of the skewness and kurtosis effects is not obvious for $\theta<70°$. Beyond this angle, the skewness and kurtosis effects contribute. The sea surface emissivity is symmetrical about $\phi=180°$ for both Gaussian and non-Gaussian slope PDFs; thus, the part for $\phi\in(180°, 360°)$ is not shown. Besides, it is also symmetrical about $\phi=90°$ for a Gaussian slope PDF, while it is not if a non-Gaussian slope PDF is considered.

The degree of polarization (DOP) of the sea surface emissivity is also calculated. It is given by (see Shaw (1999), Shaw and Marston (2000), and Li et al. (2011b) for details):

$$DOP=\frac{\varepsilon_H-\varepsilon_V}{\varepsilon_H+\varepsilon_V}. \tag{41}$$

The results are shown in Fig. 10(c) and (d). It is noticeable that the DOP is negative, which means that the intensity of the surface emission in V polarization is larger (which can be verified in 3). The absolute value of the DOP can be relatively large for large θ, e.g. it is larger than 10% for $\theta>75°$, meaning that the sea surface infrared emission is partially polarized, with over 10% energy emitted being polarized. The absolute value of the DOP is reduced after taking one reflection into account. In other words, surface reflection reduces the polarization property of the sea surface emission. The DOP also depends on the wind direction. Generally, the surface infrared emission is more polarized in the cross-wind direction than in the up-wind and down-wind directions (Fig. 10(d)).

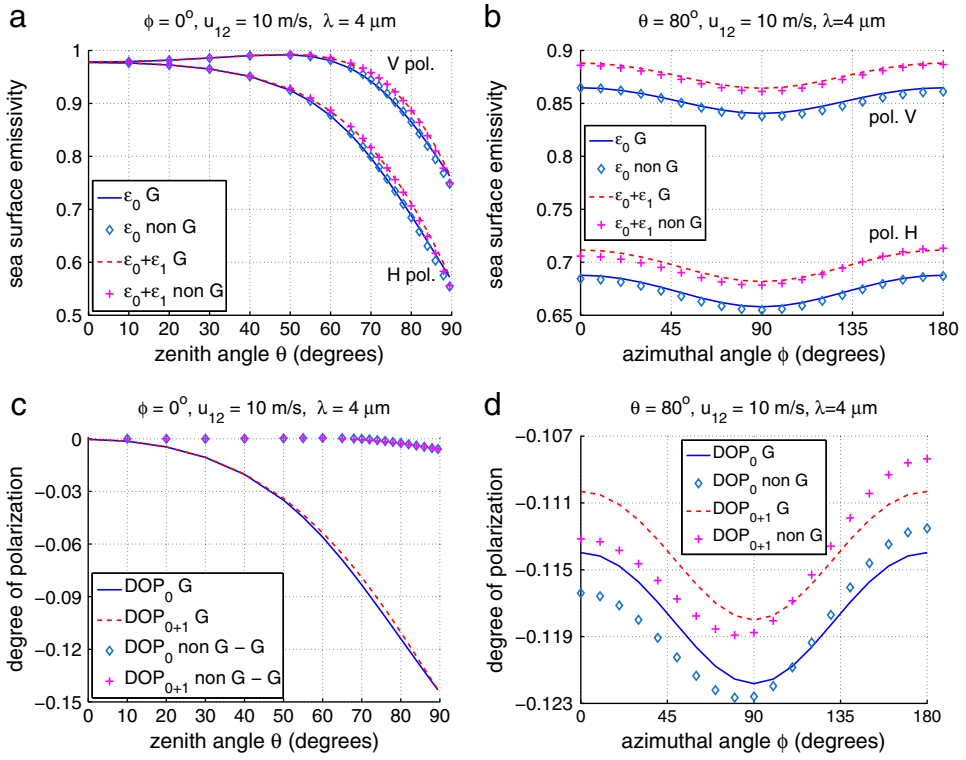

Fig. 10. The sea surface infrared emissivity and the degree of polarization (DOP) with Gaussian and non-Gaussian slope PDF with respect to θ ((a) and (c)) and ϕ ((b) and (d)). The difference of DOPs with Gaussian and non-Gaussian slope PDFs is shown in (c) as diamonds and pluses.

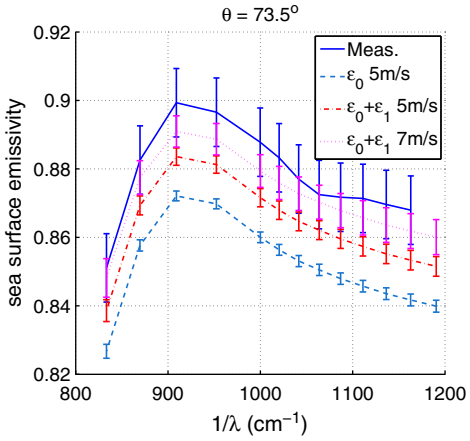

Fig. 11. Comparison of the sea surface infrared emissivity with the measurement of Smith et al. for $\theta = 73.5°$.

The DOP of surfaces with Gaussian and non-Gaussian slope PDFs are compared and their difference is calculated (see Fig. 10(c), diamonds and pluses). They are similar for $\theta < 70°$ (difference ≈ 0). Beyond this angle, the skewness and kurtosis effects contribute. For large θ, the DOP of non-Gaussian surface fluctuates with respect to the wind direction (Fig. 10(d)). Compared with Gaussian surfaces, the infrared emission of sea surfaces with non-Gaussian slope PDF is more polarized in the up-wind direction ($\phi = 0°$) and less polarized in the down-wind direction ($\phi = 180°$).

4.4. Comparison with measurements

4.4.1. Comparison with smith et al.

Smith et al. (1996) derived the sea surface infrared emissivity in the Gulf of Mexico by measurements. The measurements were carried out in January 1995. The sea surface emissivity was obtained for zenith angles $\theta = 36.5°$, 56.5° and 73.5°, whereas the azimuth angle ϕ was not specified. During the measurements, the wind speed was ranging from 2 to 8 m/s. The unpolarized emissivity was then obtained for wavelengths $\lambda \in [8,12]$ μm ($1/\lambda \in [830, 1250]$ cm^{-1}) and compared with the analytical model of Masuda et al. (1988), where no surface reflection is considered. It was shown that the measurements and the analytical result agreed well with each other for $\theta = 36.5°$ and 56.5°, but a difference over 0.02 appeared for $\theta = 73.5°$.

In this subsection, the 2D sea surface emissivity is calculated under similar conditions. The non-Gaussian surface slope PDF is used rather than the Gaussian one, as it represents better the real sea surface. Besides, the results with Gaussian and non-Gaussian PDFs are quite similar for $\theta = 73.5°$. The unpolarized sea surface emissivity is obtained by averaging the emissivities in H and V polarizations. As the azimuth angle is not specified in the measurement, an error-bar is obtained for directions $\phi = \{0°, 180°\}$ during the calculation. The wind speed is set to $u_{12} = 5$ m/s, which is the average wind speed during the measurement. The results are shown in Fig. 11. The result for $u_{12} = 7$ m/s is also shown for comparison. As the first-order emissivity is weak for $\theta = 36.5°$ and 56.5°, no significant improvement is found for these two zenith angles and the comparisons for these two angles are not shown here.

It is shown in Fig. 11 that the analytical results and the measurements have a similar form. The zero-order emissivity ε_0 underestimates the sea surface emissivity by at least 0.02. A better agreement is obtained after taking the first-order emissivity ε_1 into account. However, the analytical results still underestimate the measurements, although their error-bars overlap for some wavenumbers (around $1/\lambda \approx 1060$ cm^{-1}).

This underestimation can be attributed to several reasons. As surface emissivities with two and more surface reflections are very weak (emissivity with two reflection (SESRSR) $\varepsilon_2 \approx 0.001$ for $u_{12} = 5$ m/s, $\theta = 73.5°$, see Fig. 5 of Li et al., 2011b), taking into account higher

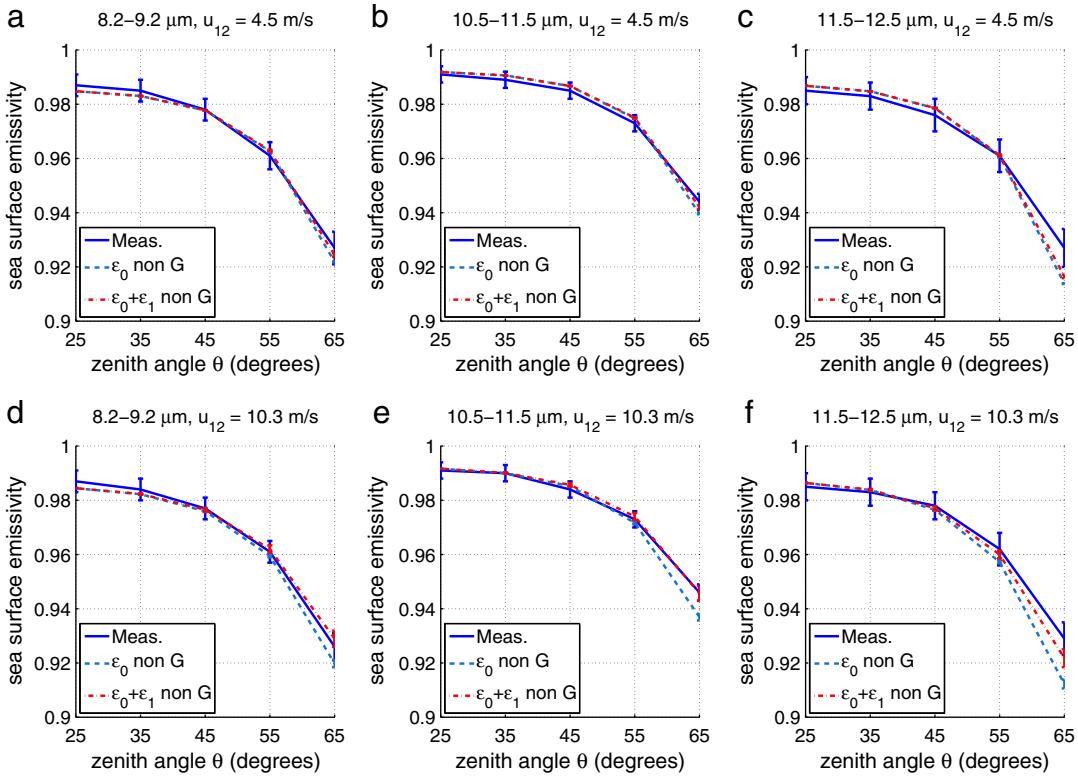

Fig. 12. Comparison of the sea surface infrared emissivity with the measurements of Niclòs et al., for channels 8.2–9.2 μm ((a) and (d)), 10.5–11.5 μm ((b) and (e)), 11.5–12.5 μm ((c) and (f)), and for wind speed $u_{12} = 4.5$ m/s ((a)–(c)) and $u_{12} = 10.3$ m/s ((d)–(f)).

orders surface reflected emissivities does not seem to reduce significantly the underestimation. One reason is that we do not take the salinity and the temperature of sea water into account (the refraction index we used is derived for fresh water at 25 °C). Another reason might be that the wind speed was not measured precisely enough. In Fig. 11, we also show the calculation result for a wind speed $u_{12}=7$ m/s, where a much better agreement is obtained.

4.4.2. Comparison with Niclòs et al.

Niclòs et al. (2005) derived the sea surface infrared emissivity of the Mediterranean sea from an oil rig above the sea surface. The measurement data are obtained for four channels of wavelengths: 8–14, 8.2–9.2, 10.5–11.5, and 11.5–12.5 μm. Measurements are carried out under two different wind speeds u_{12}, which are approximately 4.5 and 10.3 m/s. The wind direction is not specified.

To make a comparison, calculations are carried out for similar conditions. For the channel 8.2–9.2 μm, the sea surface emissivity is calculated with a step of 0.2 μm and is then averaged. For the channels 10.5–11.5 and 11.5–12.5 μm, a step of 0.5 μm is taken. An error-bar is obtained for directions $\phi=[0°, 180°]$ during the calculation. The results with non-Gaussian slope PDF are compared with measurements in Fig. 12.

Generally, the analytical result better agrees with measurements for large zenith angles ($\theta=55°$ and 65°) after taking into account the first-order emissivity contribution ε_1. In most of the cases, considering one reflection brings the analytical results into the uncertainty of measurements for $\theta=65°$ (at least error-bars overlap), except for the cases of Fig. 12(c). Even though in case of Fig. 12(c), considering one surface reflection still reduces the difference between the analytical result and the measurements.

5. Conclusion

This paper calculates the polarized infrared emissivity of the sea surface with an analytical model, where one surface reflection is considered. The analytical model expands upon the previous work Li et al. (2011b) to two-dimensional sea surfaces, thereby allowing consideration of the "cross polarization" effect. The skewness and kurtosis effects are also studied. It is shown that the agreement between the model and the measurement is greatly improved for large zenith angles by considering one surface reflection. "Cross polarization" effect in the zero-order contribution of sea surface infrared emissivity is significant for small zenith angles, but it vanishes rapidly as the zenith angle increases. "Cross polarization" effect is always weak when studying the first-order emissivity contribution. The skewness and kurtosis effects are significant for grazing zenith angles ($\theta>80°$). Sea surface infrared emissivity is sensitive to the wind direction, with $\phi=180°$ being the axis of symmetry. It is also symmetrical about $\phi=90°$ for Gaussian surfaces, whereas it is not after taking into account the skewness and kurtosis effects. For Gaussian surfaces, surface emissivity for grazing zenith angles reaches maxima in the up-wind ($\phi=0°$) and down-wind (180°) directions, whereas minima are found in the cross-wind ($\phi=90°$, 270°) directions. After taking into account the skewness and kurtosis effects, the surface emissivity has larger value in the down-wind direction ($\phi=180°$) than in the up-wind direction ($\phi=0°$).

Acknowledgement

We would like to thank the reviewers for the thoughtful reviews of our manuscript, and for the valuable and detailed comments.

Appendix A. Derivation of α

The angle α is the one between the vectors $\hat{u}_V$ and $\hat{u}_{v_0}$. By definition, the vector $\hat{u}_{v_0}$ of the local vertical polarization direction belongs to the local incidence plane defined by the local normal $\hat{n}_0$ and the observation direction $\hat{s}$, and it is perpendicular to $\hat{s}$. As a result, $\hat{u}_{v_0}$ is in the same direction as the perpendicular projection of the local normal $\hat{n}_0$ to the plane perpendicular to $\hat{s}$ (the green plane in Fig. 2)

To derive α, a new system of coordinates $x'y'z'$ is defined, with $\hat{u}_H$, $\hat{u}_V$, $\hat{s}$ being the positive x', z' and y' directions, respectively.

The system of coordinates $x'y'z'$ can be obtained by rotating firstly xyz along $\hat{z}$ clockwise through an angle $90°-\phi$, then along the new $\hat{x}'$ anticlockwise through an angle $90°-\theta$. As a result, the normal $\hat{n}_0$ in $x'y'z'$ is expressed as:

$$\hat{n}'_0 = R_x(90°-\theta)R_z(\phi-90°)\hat{n}_0, \tag{A.1}$$

where $R_x(\vartheta)$ and $R_z(\vartheta)$ are the rotation matrices, given by:

$$\begin{aligned} R_x(\vartheta) &= \begin{bmatrix} 1 & 0 & 0 \\ 0 & \cos\vartheta & -\sin\vartheta \\ 0 & \sin\vartheta & \cos\vartheta \end{bmatrix}, \\ R_z(\vartheta) &= \begin{bmatrix} \cos\vartheta & -\sin\vartheta & 0 \\ \sin\vartheta & \cos\vartheta & 0 \\ 0 & 0 & 1 \end{bmatrix}. \end{aligned} \tag{A.2}$$

The angle α becomes the one between $\hat{z}'$ and the projection of $\hat{n}'_0$ onto the $x'z'$ plane. It is given by:

$$\begin{aligned} \cos\alpha &= \frac{\left(n'_{0,x'}\hat{x}'+n'_{0,z'}\hat{z}'\right)\cdot\hat{z}'}{\|n'_{0,x'}\hat{x}'+n'_{0,z'}\hat{z}'\|\|\hat{z}'\|} \\ &= \frac{n'_{0,z'}}{\sqrt{n'^2_{0,x'}+n'^2_{0,z'}}}, \end{aligned} \tag{A.3}$$

where $n'_{0,x'}$ and $n'_{0,z'}$ are the x' and z' components of the vector $\hat{n}_0$.

The angle α can be obtained by $\alpha=\text{acos}(\cos\alpha)$, which gives a result $0°<\alpha<180°$. However, as emissivity links to intensity and the projection of intensity is considered while determining emissivity (see Eq. 10), $\sin^2\alpha$ and $\cos^2\alpha$ are involved and their signs are not important. As a result, we take the effective value $\alpha=\text{acos}(|\cos\alpha|)$ so that α never exceeds 90°.

Appendix B. Derivation of β

The angle β is the one between the local planes of incidence of the points M_0 and M_1, or equally the one between $\hat{u}_{v_1}$ and $\hat{u}_{v_0}$, or the one between $\hat{u}_{h_1}$ and $\hat{u}_{h_0}$.

With the knowledge of $\hat{s}'$ and the normals $\hat{n}_0$ and $\hat{n}_1$ of these two points, the vectors $\hat{u}_{h_1}$ and $\hat{u}_{h_0}$ are given by:

$$\begin{aligned} \hat{u}_{h_1} &= \hat{s}'\times\hat{n}_1 \\ \hat{u}_{h_0} &= \hat{s}'\times\hat{n}_0 \end{aligned}. \tag{B.1}$$

The angle β is then given by:

$$\cos\beta = \hat{u}_{h_1}\cdot\hat{u}_{h_0} \tag{B.2}$$

For the same reason as stated at the end of Appendix A, the angle β is given by its effective value $\beta=\text{acos}(|\cos\beta|)$.

Appendix C. $\Lambda(\mu)$ and $\Lambda_1(\mu_1)$

Bourlier (2005) developed analytically the non-Gaussian marginal slope PDF of the sea surface basing on the slope PDF of Cox and Munk (1954). The integrations over the slopes in Eq. (3) for $\Lambda(\mu)$ and in Eq. (19) for $\Lambda_1(\mu_1)$ are then calculated analytically.

The integration result of the function $\Lambda(\mu)$ (Eq. 3) is given by Bourlier (2005):

$$\Lambda = \Lambda_G + \alpha_S\Lambda_S + \alpha_K\Lambda_K, \tag{C.1}$$

where

$$\begin{aligned}
\upsilon &= \frac{\mu}{\sigma_X\sqrt{2}},\\
\Lambda_G &= \frac{exp\left(-\upsilon^2\right)-\upsilon\sqrt{\pi}\mathrm{erfc}(\upsilon)}{2\upsilon\sqrt{\pi}},\\
\Lambda_S &= -\frac{exp\left(-\upsilon^2\right)}{3\sqrt{2\pi}},\\
\Lambda_K &= \frac{\left(2\upsilon^2-1\right)exp\left(-\upsilon^2\right)}{6\upsilon\sqrt{\pi}},\\
\alpha_S &= \left[c_{03}(\sigma_x cos\phi)^2+3c_{21}\left(\sigma_y sin\phi\right)^2\right]\\
&\quad\times(-\sigma_X cos\phi)/\left(2\sigma_X^3\right),\\
\alpha_K &= \left[c_{04}(\sigma_x cos\phi)^4+c_{40}\left(\sigma_y sin\phi\right)^4+1.5c_{22}\sigma_x^2\sigma_y^2 sin^2(2\phi)\right]/\left(8\sigma_X^4\right).
\end{aligned} \tag{C.2}$$

Subscripts G, S and K denote "Gaussian," "skewness" and "kurtosis," respectively, and erfc(υ) is the complementary error function, and c_{21}, c_{03}, c_{04}, c_{40}, c_{22} are the skewness and kurtosis coefficients derived by Cox & Munk (1954). σ_x, σ_y and σ_X are the RMS slope of the sea surface with respect to the x, y and X directions, respectively, which is related to the wind speed u_{12} at 12.5 m above the sea surface as (Bourlier, 2005; Cox & Munk, 1954):

$$\begin{aligned}
\sigma_x^2 &= 3.16u_{12}\times10^{-3},\\
\sigma_y^2 &= 1.92u_{12}\times10^{-3}+0.003,\\
\sigma_x^2 &= (\sigma_x cos\phi)^2+\left(\sigma_y sin\phi\right)^2.
\end{aligned} \tag{C.3}$$

The non-Gaussian surface slope PDF along the direction X' can be obtained in the same way as that along X. Then, $\Lambda_1(\mu_1)$ (Eq. 19) with non-Gaussian slope PDF is given by:

$$\Lambda_1 = \Lambda_G^- + \alpha_S\Lambda_S^- + \alpha_K\Lambda_K^-, \tag{C.4}$$

where

$$\begin{aligned}
\Lambda_G^- &= -1-\Lambda_G,\\
\Lambda_S^- &= -\Lambda_S,\\
\Lambda_K^- &= -\Lambda_K.
\end{aligned} \tag{C.5}$$

$\Lambda(\mu)$ and $\Lambda_1(\mu_1)$ with Gaussian slope PDF can be obtained by setting $\alpha_S=\alpha_K=0$.

References

Bourlier, C. (2005). Unpolarized infrared emissivity with shadow from anisotropic rough sea surfaces with non-Gaussian statistics. *Applied Optics*, *44*, 4335–4349.

Bourlier, C. (2006). Unpolarized emissivity with shadow and multiple reflections from random rough surfaces with the geometric optics approximation: Application to Gaussian sea surfaces in the infrared band. *Applied Optics*, *45*, 6241–6254.

Cox, C., & Munk, W. (1954). Measurement of the roughness of the sea surface from photographs of the sun's glitter. *Journal of the Optical Society of America*, *44*, 838–850.

Freund, D. E., Joseph, R. I., Donohue, D. J., & Constantikes, K. T. (1997). Numerical computations of rough sea surface emissivity using the interaction probability density. *Journal of the Optical Society of America. A*, *14*, 1836–1849.

Hale, G. M., & Querry, M. R. (1973). Optical constants of water in the 200-nm to 200-μm wavelength region. *Applied Optics*, *12*, 555–563.

Henderson, B. G., Theiler, J., & Villeneuve, P. (2003). The polarized emissivity of a wind-roughened sea surface: A Monte Carlo model. *Remote Sensing of Environment*, *88*, 453–467.

Li, H., Pinel, N., & Bourlier, C. (2011a). Polarized infrared emissivity of one-dimensional Gaussian sea surfaces with surface reflections. *Applied Optics*, *50*, 4611–4621.

Li, H., Pinel, N., & Bourlier, C. (2011b). A monostatic illumination function with surface reflections from one-dimensional rough surfaces. *Waves in Random and Complex Media*, *21*, 105–134.

Masuda, K. (2006). Infrared sea surface emissivity including multiple reflection effect for isotropic Gaussian slope distribution model. *Remote Sensing of Environment*, *103*, 488–496.

Masuda, K., Takashima, T., & Takayama, Y. (1988). Emissivity of pure and sea waters for the model sea surface in the infrared window regions. *Remote Sensing of Environment*, *24*, 313–329.

Nalli, N. R., Minnett, P. J., & van Delst, P. (2008). Emissivity and reflection model for calculating unpolarized isotropic water surface-leaving radiance in the infrared. i: Theoretical development and calculations. *Applied Optics*, *47*, 3701–3721.

Niclòs, R., Valor, E., Caselles, V., Coll, C., & Sanchez, J. M. (2005). In situ angular measurements of thermal infrared sea surface emissivity–validation of models. *Remote Sensing of Environment*, *94*, 83–93.

Saunders, P. M. (1968). Radiance of sea and sky in the infrared window 800–1200 cm-1. *Journal of the Optical Society of America*, *58*, 645–652.

Shaw, J. A. (1999). Degree of linear polarization in spectral radiances from water-viewing infrared radiometers. *Applied Optics*, *38*, 3157–3165.

Shaw, J., & Marston, C. (2000). Polarized infrared emissivity for a rough water surface. *Optics Express*, *7*, 375–380.

Smith, B. (1967). Geometrical shadowing of a random rough surface. *IEEE Transactions on Antennas and Propagation*, *15*, 668–671.

Smith, W. L., Knuteson, R. O., Revercomb, H. E., Feltz, W., Nalli, N. R., Howell, H. B., et al. (1996). Observations of the infrared radiative properties of the ocean implications for the measurement of sea surface temperature via satellite remote sensing. *Bulletin of the American Meteorological Society*, *77*, 41–51.

Wagner, R. J. (1967). Shadowing of randomly rough surfaces. *The Journal of the Acoustical Society of America*, *41*, 138–147.

Watts, P. D., Allen, M. R., & Nightingale, T. J. (1996). Wind speed effects on sea surface emission and reflection for the along track scanning radiometer. *Journal of Atmospheric and Oceanic Technology*, *13*, 126–141.

Wu, X., & Smith, W. L. (1997). Emissivity of rough sea surface for 8–13 μm: Modeling and verification. *Applied Optics*, *36*, 2609–2619.

Yoshimori, K., Itoh, K., & Ichioka, Y. (1994). Thermal radiative and reflective characteristics of a wind-roughened water surface. *Journal of the Optical Society of America. A*, *11*, 1886–1893.

Yoshimori, K., Itoh, K., & Ichioka, Y. (1995). Optical characteristics of a wind-roughened water surface: A two-dimensional theory. *Applied Optics*, *34*, 6236–6247.